PHYSICS

Sensitivity of Susceptibility-Weighted Imaging in Detecting Superparamagnetic Iron Oxide-Labeled Mesenchymal Stem Cells: A Comparative Study

Serah Park [1]; Byung Kook Kwak [1,2,*]; Jisung Jung [1]

[1]Department of Radiology, Chung-Ang University College of Medicine, Seoul, Korea
[2]Department of Radiology, Chung-Ang University Hospital, Chung-Ang University College of Medicine, Seoul, Korea

Corresponding author: Byung Kook Kwak, Department of Radiology, Chung-Ang University Hospital, Chung-Ang University College of Medicine, P. O. Box: 156-755, Seoul, Korea. Tel: +82-262992661, Fax: +82-262631557, E-mail: kwakbk@cau.ac.kr

Background: Susceptibility-weighted imaging (SWI) is extremely sensitive in the detection of superparamagnetic iron oxide (SPIO) nanoparticle-labeled cells. However, no study has compared molecular imaging for stem cell detection using SWI and other MRI pulse sequences.

Objectives: This study aims to assess the sensitivity of SWI in detecting SPIO nanoparticle-labeled, human bone marrow-derived mesenchymal stem cells (SPIO-hMSCs) compared with that of T_2- and T_2*-weighted imaging (T_2WI and T_2*WI, respectively) in a phantom and in vivo study in rats.

Materials and Methods: A phantom was prepared with various cell concentrations. In one normal rat, SPIO-hMSCs were implanted directly through burr holes into both caudate putamens, while in three rats without and six rats with photothrombotic infarction, 2.5×10^5/ml SPIO-hMSCs were infused into the ipsilateral internal carotid artery (ICA). T_2WI, T_2*WI, and SWI findings were compared for dark regions representing SPIO-hMSCs.

Results: SWI and T_2*WI detected 15 µL of 13 SPIO-hMSCs/µL and 15 µL of 27 SPIO-hMSCs/µL in the phantom, respectively and 3 µL of 333 SPIO-hMSCs/µL and 3 µL of 167 SPIO-hMSCs/µL in the normal rat brain (direct implantation). In the normal rat brain (ICA infusion), one of the three cases showed numerous foci of dark regions dispersed throughout the brain on T_2*WI and SWI. Dark regions surrounded the infarcts in all six infracted rat brains. The dark region was most prominent on SWI, followed by T_2*WI and T_2WI in all six rats (P = 0.002). Implanted SPIO-hMSCs were confirmed using Prussian blue staining.

Conclusions: SWI is the most sensitive in the detection of SPIO-hMSCs, with the dark regions representing SPIO-hMSCs being more prominent on SWI than on T_2*WI and T_2WI.

Keywords: Mesenchymal Stromal Cells; Cerebral Infarction; Rats; Ferrosoferric Oxide

1. Background

Superparamagnetic iron oxide (SPIO) nanoparticles are used as contrast agents in T_2-weighted magnetic resonance imaging (MRI) because of their ability to decrease the T_2 relaxation time. Areas containing SPIO nanoparticles appear dark on T_2-weighted imaging (T_2WI) and T_2*-weighted imaging (T_2*WI) because SPIO nanoparticles decrease the signals originating from protons by fast proton dephasing, i.e. the susceptibility effect (1-3). Any SPIO nanoparticle-labeled cells can be tracked by MRI (4-8), which has the highest resolution among molecular imaging modalities. However, with respect to sensitivity in the detection of fewer cells, MRI is not superior to optical imaging. Therefore, cell detectability using MRI needs improvement, specifically by choosing the optimal pulse sequence. The most sensitive SPIO-labeled cell detection can be achieved by utilizing MRI pulse sequences that maximize its sensitivity to the susceptibility effect of SPIO nanoparticles, i.e. T_2WI and T_2*WI (9). Susceptibility-weighted imaging (SWI) is extremely sensitive to subtle changes and offers optimal detection for SPIO-labeled cell. It involves a three-dimensional (3D), fully flow-compensated, gradient-echo sequence with a long echo time (TE) (10, 11). However, till date, no study has compared molecular imaging for stem cell detection using SWI and that using other MRI pulse sequences (12).

2. Objectives

This study aimed to assess the sensitivity of SWI in the detection of SPIO nanoparticle-labeled, human bone marrow-derived mesenchymal stem cells (SPIO-hMSCs) compared with that of T_2WI and T_2*WI in a phantom and in vivo study.

3. Materials and Methods

3.1. Cell Preparation and Labeling

Mesenchymal stem cells derived from human bone marrow (hMSCs; Lonza, Walkersville, MD, USA) were grown in Dulbecco's modified Eagle's medium (DMEM) containing 10% fetal bovine serum, 200 mM L-glutamine, and 0.1 mg/mL gentamicin (all Invitrogen, Carlsbad, CA, USA) at 37°C in 5% CO_2. Culture media were changed every 3-4 days, and the cells were subcultured at 80%-90% confluency. hMSCs labeling with SPIO nanoparticles was performed at approximately 80% confluency. To enable efficient internalization of SPIO nanoparticles into hMSCs, 1.5 μg/mL poly L-lysine hydrobromide (PLL; Sigma, St Louis, MO, USA) as the transfection agent and 100 μg Fe/mL SPIO nanoparticles (Feridex IV; Advanced Susceptibility Inc., Cambridge, MA, USA) were combined in culture medium and gently shaken for 60 min at room temperature on a rotating shaker. hMSCs were supplied with culture media containing the SPIO-PLL complex at a final concentration of 50 μg Fe/mL SPIO nanoparticles and 750 ng/mL PLL to ensure efficient labeling (6). The cell cultures were kept overnight at 37°C in 5% CO_2. Prussian blue staining was used to confirm successful and effective hMSC labeling. The cells labeled in 4-chamber slides (Lab-Tek; Electron Microscopy Science, Hatfield, PA, USA) were washed twice with phosphate-buffered saline (PBS) to remove excess unlabeled SPIO nanoparticles, fixed with 4% paraformaldehyde for 30 min, washed again, and incubated with 2% potassium ferrocyanide in 2% hydrochloric acid for 30 min. After another PBS wash, the cells were counterstained with nuclear fast red. The SPIO labeling efficiency was microscopically observed.

3.2. Cell Phantom

SPIO-hMSCs were harvested by cell dissociation reagent (TrypLE Express, Invitrogen) treatment for 5 min. SPIO-hMSCs were washed with the medium and centrifuged to obtain a 200-cell/μL concentration. To prepare cell phantoms of various concentrations, the cells were diluted to concentrations of 20, 40, 80, 120, 160, and 200 cells/μL in the medium. Furthermore, 2% agarose (Invitrogen) was prepared in distilled water. Five microliters of each cell concentration and 10 μL of 2% agarose solution were mixed in a 1:2 ratio. Cell-agarose gel lumps were prepared. To prepare the phantom, 180 μL of 2% agarose solution was poured at the bottom of the 96-well plate, the lumps were placed in the center of the agarose gel, and 120 μL of 2% agarose solution was added. Eight wells were linearly prepared, i.e. 15-μL volume lumps of only 2% agarose; 7, 13, 27, 40, 53, and 67 SPIO-hMSCs/μL; and 67 unlabeled hMSCs/μL. Phantom preparation and MR imaging (the protocol will be mentioned later) were replicated five times.

3.3. Animal Experiments

The study protocol was approved by the institutional review board (CAUMD 11-0020), and the rats were maintained as per the Institutional Animal Ethics Committee at Chung-Ang University. Before the experiment, the rats were allowed to acclimatize for a week in a room under a 12-h light/dark cycle at 21-24 °C and were fed standard rat food and tap water ad libitum. Nine male Sprague Dawley rats (Daehan Biolink, Eumseong, Korea), each weighing 250-300 g, were used.

3.4. Direct Implantation into Normal Rat Brains

SPIO-hMSC cell suspensions at two cell concentrations, i.e. 3 μL of 333 SPIO-hMSCs/μL in serum-free medium for the right brain and 3 μL of 167 SPIO-hMSCs/μL for the left brain, were loaded into a Hamilton syringe (Hamilton Co, Reno, NV, USA) with a 25-G needle. Three rats received intramuscular anesthesia with 50 mg/kg body weight Zoletil 50 (Virbac S.A, Carros, France) and 10 mg/kg Rompun (Xylazine hydrochloride; Bayer Korea, Ansan, Korea). Rat heads were fixed in the stereotactic system (Stoelting, Wood Dale, IL, USA). The scalp skin was centrally incised and two burr holes were constructed on each side of the skull at 0.48 mm posterior to the bregma and 3.4 mm from the mid-line sagittal suture. The needle was inserted to a 6.4-mm depth into the caudate putamen using the stereotactic system. Cells were slowly injected into both caudate putamens for 3 min and the needle was kept in position for 10 min. MRI (protocol will be mentioned later) was performed after an hour. The rats were sacrificed (protocol will be mentioned later) and their brains were harvested and fixed for histopathological studies.

3.5. Internal Carotid Artery (ICA) Infusion in Normal Rats and Rat Models with Cerebral Infarction

SPIO-hMSCs were infused into the ICA of three normal rats and six rats with local brain infarction. To induce photothrombotic cerebral infarction (PTCI) (13, 14), the rats were anesthetized with 5% isoflurane (Aerane Solution, Ilsung, Seoul, South Korea) in O_2 that was maintained with 1.5%-2% isoflurane. The rats were laid flat in the prone position with their heads fixed in the stereotactic system (Stoelting, Wood Dale, IL, USA). A midline scalp incision was placed and a fiberoptic cold light generator guide (Fiber-Lite MI-150; Dolan Jenner Co., Lancaster, SC, USA) with a 5-mm aperture was positioned on the skull, 2.5 mm right lateral to the midline and 2.5 mm posterior to the bregma. The wavelength of the light was 400-670 nm, and its color temperature was 3200°K. Following intravenous Rose Bengal (20 mg/kg; Sigma-Aldrich Co, St. Louis, MO, USA) injection through the tail vein, photoillumination was performed for 15 min, which generated free radicals from Rose Bengal, endothelial cell damage, platelet aggregation leading

to microvascular thrombosis, and eventually, vessel occlusion with circumscribed cortical infarction. The scalp was sutured with 4-0 blue-nylon and the rats were allowed to recover. During this procedure, the rectal temperature was monitored using the homeothermic blanket control unit (Harvard Apparatus, Holliston, MA, USA) and maintained between 36.5°C and 37°C with a feedback-controlled heating pad. Three days following photothrombotic infarction, SPIO-hMSCs were infused into the ipsilateral right ICA. Rats were anesthetized by intramuscular injection of 100 mg/kg body weight Ketara (Ketamine hydrochloride; Yuhan, Seoul, Korea) and 10 mg/kg Rompun (Xylazine hydrochloride; Bayer Korea, Ansan, Korea). The ipsilateral carotid artery was exposed and the external carotid artery was ligated with 6-0 silk, and 2.5×10^5 SPIO-hMSCs were injected into ICA through the common carotid artery using a 27-G needle (Introcan Certo; B Braun Melsungen AG, Melsungen, Germany). The common carotid artery was ligated with silk and the skin was closed. After 24 h, MRI (protocol will be described later) was performed, following which the rats were sacrificed (protocol will be described later) and their brains harvested and fixed for histopathological study.

3.6. Phantom MRI

Using a 3.0-T clinical MRI scanner (Achieva; Philips Healthcare, Eindhoven, The Netherlands) and the SENSE-8 channel head coil (Philips Healthcare), T_2WI (turbo spin echo; repetition time [TR] 818.7 ms; TE, 80 ms; flip angle, 90°C; field of view, 180 × 180 mm; matrix size, 504 × 445, two-dimensional [2D] thickness, 1 mm; 8 excitations; resolution, 0.36 × 0.4 × 1.0 mm), T2*WI (gradient echo; TR, 262.4 ms; TE, 9.2 ms; flip angle, 30°C; field of view, 180 × 180 mm; matrix size, 488 × 485; 2D; thickness, 1 mm; 8 excitations; resolution, 0.37 × 0.37 × 1.0 mm), and SWI (TR, 33.1 ms; TE, 43.1 ms; flip angle, 10°; field of view, 180 × 180 mm; matrix size, 344 × 350; 3D; thickness, 1 mm; 8 excitations; resolution, 0.52 × 0.51 × 0.5 mm) were performed. A radiologist (B.K.K, one of the authors) with 23 years of experience interpreted the images with respect to the detection and size of dark regions.

3.7. In Vivo Rat Brain MRI

In vivo rat brain MRI was performed using a 3.0-T clinical MRI scanner (Achieva; Philips Healthcare) and the SENSE Wrist-4 channel coil (Philips Healthcare). Coronal brain images were obtained with rats in the prone position. The MR protocol included T2WI (TR, 4279 ms; TE, 80 ms; flip angle, 90°C; field of view, 50 × 50 mm; matrix size, 200 × 200; 2D; slice thickness, 1 mm; 3 excitations; resolution, 0.25 × 0.25 × 1.0 mm), T_2*WI (TR, 713 ms; TE, 23 ms; flip angle, 18°C; field of view, 50 × 50 mm; matrix size, 200 × 200; 2D; slice thickness, 1 mm; 3 excitations; resolution, 0.25 × 0.25 × 1.0 mm), and SWI (TR, 31.6 ms;

TE, 44.1 ms; flip angle, 15°C; field of view, 50 × 50 mm; matrix size, 128 × 128; 3D; slice thickness, 0.5 mm; 3 excitations; resolution, 0.39 × 0.39 × 0.5 mm).

3.8. MRI Analysis

MR images of six PTCI rats intra-arterially infused with SPIO-hMSCs were analyzed using picture archiving and communication system (PACS; Maroview version 5.3; Marotech, Seoul, Korea). A radiologist (B.K.K) assessed successful cerebral infarction induction, occurrence of any abnormal changes due to ICA infusion of SPIO-hMSCs, and distribution of dark regions derived from SPIO-hMSCs by comparing the images one by one with the stained slides. The dark regions were graded depending on the amount and pattern of distribution around each cerebral infarct. A strong and continuous distribution surrounding the cerebral infarct was graded as +++. A dark region completely surrounding the cerebral infarct, which was not remarkable or did not completely surround the cerebral infarct with remarkable amounts was graded as ++. A dark region weakly surrounding the cerebral infarct, which had a light band or did not completely surround the cerebral infarct with unremarkable amounts was graded as +. Only marks surrounding the cerebral infarct were graded as +/ − and absence of marks surrounding the cerebral infarct was graded as −. Statistical analysis was performed using Pearson's chi-square test with SPSS version 12.0 (SPSS Inc., Chicago, IL, USA). A P-value less than 0.05 was considered statistically significant.

3.9. Tissue Extraction and Pathology

The rats were anesthetized by intramuscular injection of 50 mg/kg body weight Zoletil 50 (Virbac S.A) and 10 mg/kg Rompun (Bayer Korea). The rats were perfused through the heart with 200 mL of 5 U/mL heparinized physiological saline followed by 200 mL of 4% paraformaldehyde solution. Rat brains were harvested, fixed in 4% paraformaldehyde solution, and embedded with paraffin. Paraffin block sections with a 5-μm thickness were immersed in xylene and ethanol solution for deparaffinization and rehydration. Hematoxylin and eosin (HE) staining was performed. After washing with distilled water, the sections were stained in the hematoxylin and eosin solutions for 8 and 1 min, respectively. Anatomic orientation, ischemic necrosis, inflammation, and hemorrhage were evaluated. Prussian blue staining was performed for the detection of iron from SPIO nanoparticles in hMSCs. Slides were placed in a Coplin jar containing a 1:1 mixture of 2% potassium ferricyanide and 1% hydrochloric acid for 30 min at room temperature. They were then rinsed well with distilled water and counterstained with nuclear fast red (Vector Laboratories, Burlingame, CA, USA) for 5 min. Comparing the stained slides one by one with the MR images, SPIO-hMSCs were evaluated with focus on distribution.

4. Results

Prussian blue staining of SPIO-labeled hMSCs showed that 100% cells were labeled with SPIO without any cell damage (Figure 1). T_2WI did not detect SPIO-hMSCs in the phantom, even in the highest concentration of 67 SPIO-hMSCs/μL (Figure 2). T_2*WI showed dark regions in cell lumps of 15 μL of 27, 40, 53, and 67 SPIO-hMSCs/μL. On SWI, cell lumps of 15 μL of 13, 27, 40, 53, and 67 SPIO-hM-SCs /μL showed dark regions. SWI detected a lump with a lower concentration of 13 SPIO-hMSCs/μL compared with T_2*WI, which detected a lump of 27 SPIO-hMSCs/μL. In all the pulse sequences, lumps not containing cells (only 2% agarose) and lumps of 15 μL of 67 unlabeled hM-SCs/μL did not show any dark regions. The dark regions on SWI were of an exaggerated intensity and were larger than those on T_2*WI for the same lump.

In normal rat brain MRI, performed an hour after direct SPIO-hMSC implantation, T_2WI did not show any dark regions (Figure 3 A). On T_2*WI and SWI, 3 μL of 333

Figure 2. MRI of the phantom with eight wells. Each well has a 15-μL lump of superparamagnetic iron oxide-labeled human bone marrow-derived mesenchymal stem cells (SPIO-hMSCs) in different concentrations: no cells; 7, 13, 27, 40, 53, and 67 SPIO-hMSCs/μL; and 67 unlabeled hMSCs/μL. T_2-weighted imaging (T_2WI) does not detect SPIO-hMSCs even in the highest concentration of 67 SPIO-hMSCs/μL. T_2*-weighted imaging (T_2*WI) shows a dark region for cell lumps in 15 μL of 27, 40, 53, and 67 SPIO-hMSCs/μL. On susceptibility-weighted imaging (SWI), cell lumps in 15 μL of 13, 27, 40, 53, and 67 SPIO-hMSCs/μL show dark regions. SWI detects a lump of a lower concentration of 13 SPIO-MSCs/μL compared with T_2*WI, which detects a concentration of 27 SPIO-MSCs/μL. The dark regions on SWI are more intense and larger in size than those on T_2*WI for the same lump. The bulls-eyes indicate air bubble artifacts.

SPIO-hMSCs/μL (right caudate putamen) and 3 μL of 167 SPIO-hMSCs/μL (left caudate putamen), respectively, were noted as dark regions on each brain side. The size of the dark region was bigger in 333 SPIO-hMSCs/μL than in 167 SPIO-hMSCs/μL. The dark regions in both caudate putamens were larger and more prominent on SWI than on T_2*WI (Figure 3 A). The implanted cells were confirmed on each side by Prussian blue staining (Figure 3 B).

In the normal rat brain MRI performed 24 h after ICA infusion, one of the three rats (33%) showed numerous foci of dark regions dispersed throughout the brain on T_2*WI and SWI (Figure 3 C), while the other two did not show any dark regions. On Prussian blue staining, these foci were confirmed to be SPIO-hMSCs in the whole brain (Figure 3 D). The foci were more prominent on SWI than on T_2*WI; however, they were not observed on T_2WI (Figure 3 C). The reason for the development of these foci in both cerebral hemispheres of the rats was considered to be a patent circle of Willis.

On MRI, which was obtained 24 h after ICA infusion with SPIO-hMSCs, focal and oval photothrombotic cerebral infarctions were observed in the right frontoparietal lobe in all six rats with high signal intensity on T_2WI, T_2*WI, and SWI (Figure 4 A and 4C). Dark regions surrounding the cerebral infarcts were noted, which were most prominent on SWI, followed by T_2* WI and T_2WI in all six rats (Table 1) (Figure 4 A and 4C). The trend analysis was statistically significant (P = 0.002). The dark regions occurred because of migration of SPIO-hMSCs through ICA into the surrounding infarction, i.e. engraftment (15). Engraftment was confirmed by Prussian blue staining in all six
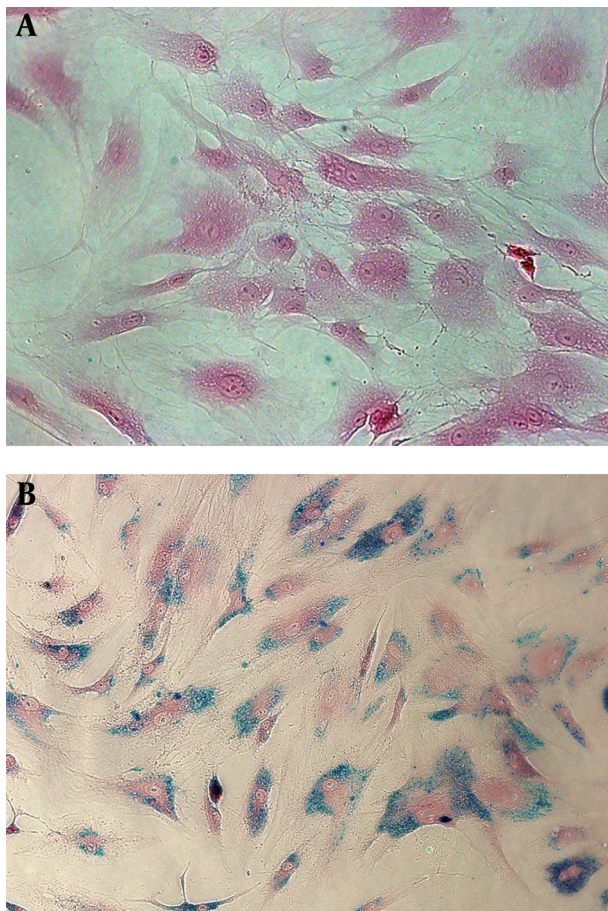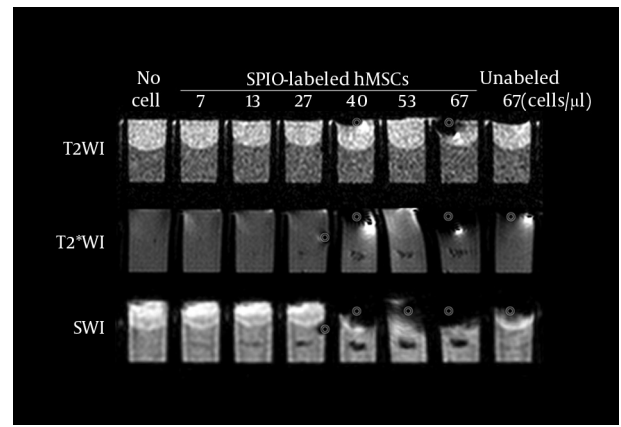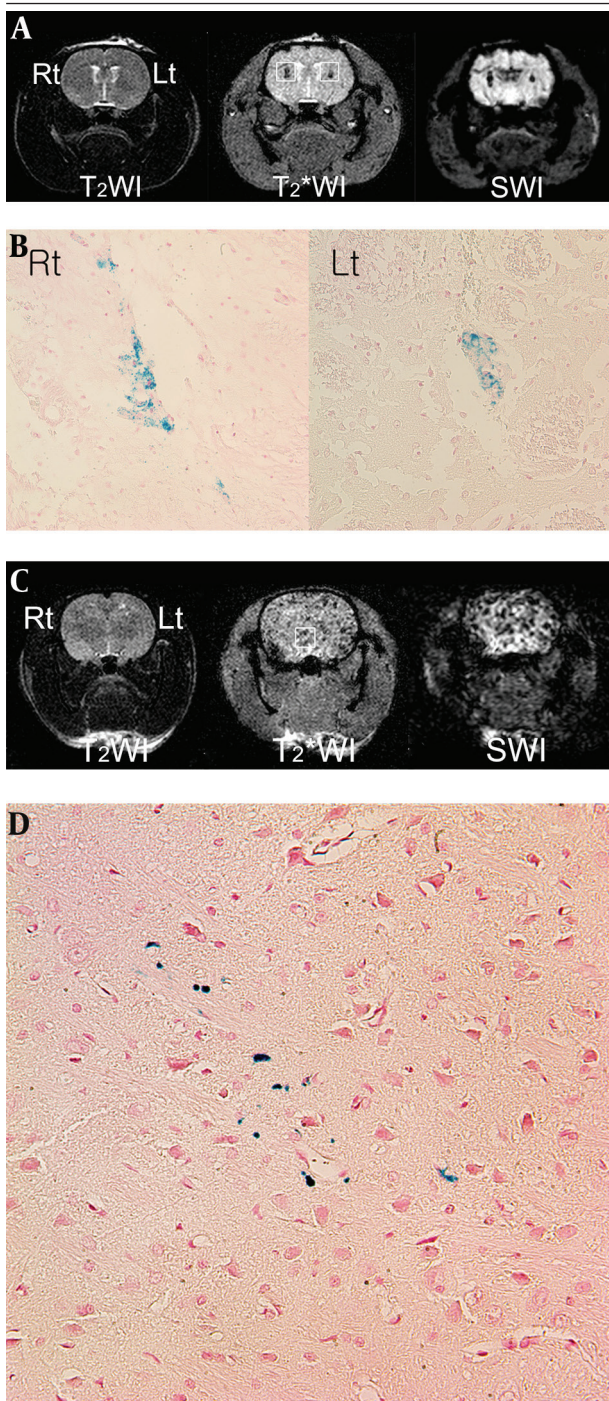

Figure 1. Prussian blue staining of unlabeled human bone marrow. Derived mesenchymal stem cells (hMSCs). A, superparamagnetic iron oxide (SPIO)-labeled hMSCs. B, All hMSCs are sufficiently labeled with SPIO nanoparticles without any cell damage in the medium containing 50 μg Fe/mL of SPIO nanoparticles and 750 ng/mL poly L-lysine (magnification, ×200).

Figure 3. Superparamagnetic iron oxide-labeled human bone marrow. Derived mesenchymal stem cell (SPIO-hMSC) detection using magnetic resonance imaging (MRI) 1 h after direct implantation (A) and 24 h after intra-arterial implantation (C) in the normal rat brain T_2-weighted imaging (T2WI) does not detect SPIO-hMSCs (A, C). On T_2*-weighted imaging (T_2*WI) and susceptibility-weighted imaging (SWI), the dark region in the right caudate putamen implanted with 3 μL of 333 SPIO-hMSCs/μL is larger than that in the left caudate putamen implanted with 3 μL of 167 SPIO-hMSCs/μL (A, squares). The dark regions are larger and more prominent on SWI than on T_2*WI (A). On normal rat brain T_2*WI and SWI, numerous foci of dark regions are dispersed throughout the brain (C, square), probably because the rat has a patent circle of Willis. On Prussian blue staining, the dark regions are confirmed to be SPIO-hMSCs (B, D) (magnification, × 400).
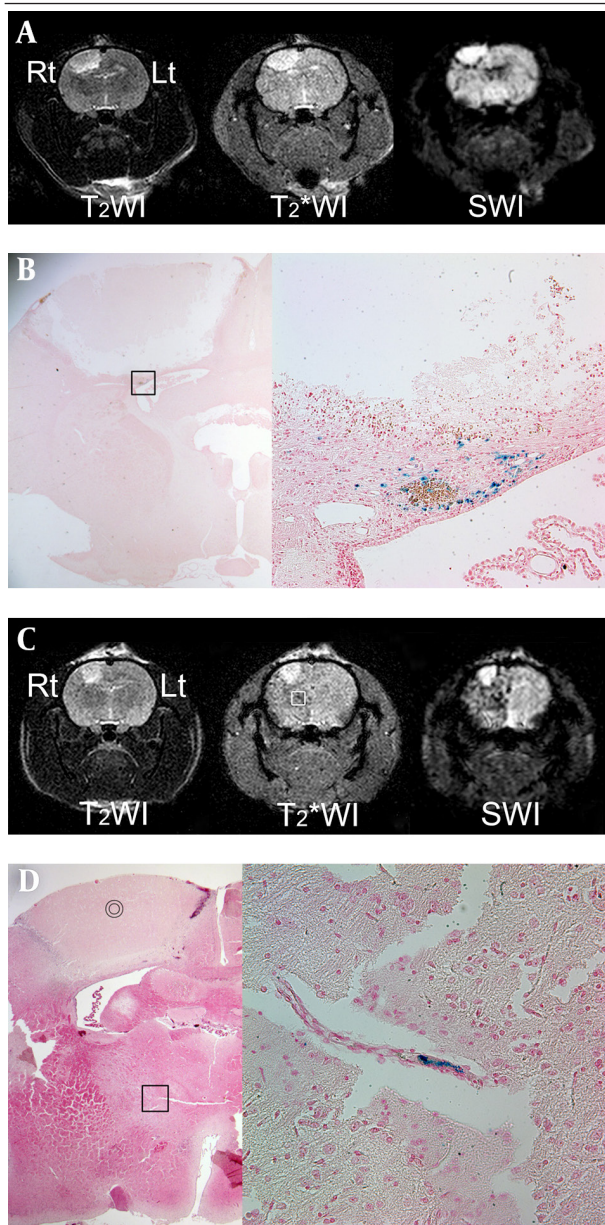

Figure 4. MRI performed 24 h after intra-arterial superparamagnetic iron oxide-labeled human bone marrow-derived mesenchymal stem cell (SPIO-hMSC) infusion in rats with photothrombotic cerebral infarction. Focal and oval cerebral infarctions are induced in the right frontoparietal lobe, with high signal intensity on T_2-weighted imaging (T_2WI), T_2*-weighted imaging (T_2*WI), and susceptibility-weighted imaging (SWI) (A, C). Dark regions surrounding the cerebral infarct are confirmed as engrafted SPIO-hMSCs by Prussian blue staining (magnification, × 12.5 and × 400) (B; square). Other foci of dark regions are dispersed in the right hemisphere, particularly on SWI, and they are not remarkable even on T_2*WI (C, square). The bullseyes indicate cerebral infarction on hematoxylin and eosin staining (magnification, × 12.5) (D). The foci of dark regions are identified as SPIO-hMSCs plugging the cerebral artery by Prussian blue staining (magnification, × 400; D; square).

rats (Figure 4 B). Meanwhile, foci of dark regions in the ipsilateral cerebral hemisphere in two rats (33%) were distinctly observed on SWI, faintly observed on T_2*WI, and not observed on T_2WI (Figure 4 C). These foci, which developed because of plugging of some small arteries by SPIO-hMSCs, were identified by Prussian blue staining (Figure 4 D).

Table 1. Qualitative Assessment for SPIO-hMSCs Distribution by Infarction on MRI

No.	Location of the Infarction	Dark Regions Around the Infarct [a,b]			Remark
		T_2WI	T_2^*WI	SWI	
1	Rt. frontoparietal	−	+	++	
2	Rt. frontoparietal	−	+/ −	+++	Numerous dark foci in the right hemisphere
3	Rt. frontoparietal	+/ −	+	++	
4	Rt. frontoparietal	+/ −	+	++	Numerous dark foci and consequent changes in the right hemisphere
5	Rt. frontoparietal	−	+/ −	++	
6	Rt. frontoparietal	−	+/ −	+	

[a] Grades of dark regions around each cerebral infarct: strong and continuous distribution (+++); complete, but not remarkable or remarkable, but not complete (++); not complete and unremarkable (+); only marks (+/ −); and no marks (−).
[b] Dark regions surrounding the cerebral infarcts on magnetic resonance imaging performed 24 h after intra-arterial infusion of superparamagnetic iron oxide-labeled human bone marrow-derived mesenchymal stem cells (SPIO-hMSCs) are most prominent on susceptibility-weighted imaging (SWI), followed by T_2^*-weighted imaging (T_2^*WI) and T_2-weighted imaging (T_2WI) in six rats. The trend analysis is statistically significant (P = 0.002).

5. Discussion

This phantom study comparing T_2WI, T_2^*WI, and SWI demonstrated that SWI is the most sensitive in SPIO-hMSC detection. T_2WI did not detect SPIO-hMSCs in the cell concentration range used in this study. SWI detected a lump of fewer cells of 13 SPIO-hMSCs/μL compared with T_2^*WI, which detected a lump of 27 SPIO-hMSCs/μL (Figure 2). It is difficult to compare the sensitivity obtained in this study with that in other studies because of differences in magnet strength (e.g. 4.7 T vs. 9.4 T) among individual MRI machines, in pulse sequences used for imaging (e.g. spin echo vs. gradient echo; differences in resolution), and in types of cell preparations (e.g. prepared cell number and volume). In a study using 17.6-T MRI with the gradient echo technique, the fewest cells were detected (2 μL of 50/μL, 100 cells) (16). In another phantom study using 9.4-T and 4.7-T MRI with the same phantom and imaging parameters, 9.4-T MRI (gradient echo) was superior in detecting the SPIO-labeled neural stem cells in a concentration of 1×10^2 cells (volume unknown) compared with 4.7-T MRI (gradient echo), which detected cells in a concentration of 5×10^2 cells (volume unknown) (17). They used 2% gelatin blocks containing SPIO-labeled neural stem cells for the phantom, similar to that used in the present study. The minimal number of cells detected was also similar to that in the present study, in which 15 μL of 27 SPIO-hMSCs/μL (400 cells) were detected on 3.0-T T_2^*WI. Meanwhile, no information is available regarding the minimum cell concentration that can be detected using SWI. In the present study, 3.0-T SWI detected 15 μL of 13 SPIO-hMSCs/μL (200 cells). SWI was used only in one of the several studies performed using MRI for molecular imaging. Cheng et al. first used the SWI pulse sequence for SPIO-hMSCs (12). However, they did not mention the minimal cell number that can be detected using SWI. The size of the dark region derived from SPIO-hMSCs was larger on SWI than on T_2^*WI in the phantom and in the direct and ICA infusion studies of the rat brain (Figures 2 - 4). The size of the dark regions was increased on SWI. Some reports have mentioned the increase in volume on SWI compared with that in the real sample. In the study by Mittal et al. and Babikian et al. SWI was 3-6 times more sensitive than conventional T_2^*WI in detecting the size, number, volume, and distribution of hemorrhagic lesions after cerebral injury (10, 18). It may be easy to detect SPIO-hMSCs on SWI because of the increased intensity of dark regions.

At 24 h after ICA infusion in six rats with photothrombotic cerebral infarction, engrafted SPIO-hMSCs were detected around the cerebral infarction (6/6, 100%) on MRI (Figure 4). ICA infusion is very effective in delivering stem cells to the lesion, particularly in the early phase after infusion (15, 19, 20). T_2WI did not detect SPIO-hMSCs observed as dark regions in other sequences. The surrounding dark regions were more prominent on SWI than on T_2^*WI. Meanwhile, SPIO-hMSCs were also detected and distributed in the whole ipsilateral normal parenchyma (2/6, 33%) (Figure 4) (15, 21) probably because of plugging of end arteries in the cerebrum that led to infarction (Figure 3 C and 4C). The dark regions caused by plugging of end arteries were also more distinct on SWI than on T_2^*WI. However, plugging of the end artery is suspected to be developed only in a small animal study because of the relatively small cerebral artery caliber. In humans, plugging of end arteries cannot be suspected because of the large cerebral artery caliber and some other techniques that prevent dispersed cell aggregation. The cells infused into one side of the brain are distributed to the contralateral side (Figure 3 C) probably because of a patent circle of Willis. This phenomenon is also not critical to humans because small-caliber arteries distal to the circle of Willis can be superselected.

SWI has drawbacks, such as artifacts, which are not frequent with other MRI pulse sequences (Figures 2 - 4). SWI can detect non-uniformity of local magnetic fields

caused by paramagnetic and diamagnetic tissues (11, 22, 23). Paramagnetic materials always demonstrate low signal intensity on magnitude and phase images, while diamagnetic materials demonstrate high signal intensity on phase images and low signal intensity on magnitude images (24). Therefore, when interpreting SWI findings, paramagnetic materials that can result in dark signal artifacts, such as deoxygenated venous blood, hemorrhage, iron, and air, should be ruled out (10, 11).

This study has limitations. First, because of the indirect detection of cells through the SPIO effect on proton relaxation, it was difficult to absolutely quantify the cell concentration (25). Second, it was difficult to discriminate SPIO-labeled cells in areas of hemorrhage and traumatic injury because of proton dephasing effects of methemoglobin, ferritin, and hemosiderin, particularly at higher fields. There is a possibility of occasional misinterpretation of isolated dark regions because of differences in magnetic susceptibility around blood vessels and air-tissue interfaces (i.e. stomach and gastrointestinal tract). Third, in the in vivo study, there was no exact correlation between MRI and the actual cell number. Researchers only know the number of infused cells and not the number of imaged cells. Fourth, the number of rats included in this study was too small. Therefore, a further study with more rats is warranted. For practical applications, the labeling of cells with SPIO nanoparticles and MRI are expected to effectively track the cells in the human (26). Because the resolution of MR images is much lower in humans than in small animals, the most sensitive pulse sequence is undoubtedly needed. Based on this animal study, it will make human trial successful with SWI pulse sequence.

In conclusion, SWI is the most sensitive in the detection of SPIO-hMSCs compared with T_2*WI and T_2WI, with the dark regions representing SPIO-hMSCs being more prominent on SWI than on the other two pulse sequences.

Acknowledgements

Authors' Contributions

Study concept and design: Serah Park, Byung Kook Kwak, and Jisung Jung. Analysis and interpretation of data: Serah Park, Byung Kook Kwak, and Jisung Jung. Drafting of the manuscript: Serah Park. Critical revision of the manuscript for important intellectual content: Serah Park, Byung Kook Kwak, and Jisung Jung. Statistical analysis: Byung Kook Kwak, and Jisung Jung.

References

1. Long CM, Bulte JW. In vivo tracking of cellular therapeutics using magnetic resonance imaging. *Expert Opin Biol Ther.* 2009;**9**(3):293–306.

2. Bulte JW. In vivo MRI cell tracking: clinical studies. *AJR Am J Roentgenol.* 2009;**193**(2):314–25.

3. Bulte JW, Kraitchman DL. Iron oxide MR contrast agents for molecular and cellular imaging. *NMR Biomed.* 2004;**17**(7):484–99.

4. Mohammadi-Nejad AR, Hossein-Zadeh GA, Soltanian-Zadeh H. Quantitative evaluation of optimal imaging parameters for single-cell detection in MRI using simulation. *Magn Reson Imaging.* 2010;**28**(3):408–17.

5. Hu SL, Lu PG, Zhang LJ, Li F, Chen Z, Wu N, et al. In vivo magnetic resonance imaging tracking of SPIO-labeled human umbilical cord mesenchymal stem cells. *J Cell Biochem.* 2012;**113**(3):1005–12.

6. Reddy AM, Kwak BK, Shim HJ, Ahn C, Cho SH, Kim BJ, et al. Functional characterization of mesenchymal stem cells labeled with a novel PVP-coated superparamagnetic iron oxide. *Contrast Media Mol Imaging.* 2009;**4**(3):118–26.

7. Wang L, Deng J, Wang J, Xiang B, Yang T, Gruwel M, et al. Superparamagnetic iron oxide does not affect the viability and function of adipose-derived stem cells, and superparamagnetic iron oxide-enhanced magnetic resonance imaging identifies viable cells. *Magn Reson Imaging.* 2009;**27**(1):108–19.

8. Liu W, Frank JA. Detection and quantification of magnetically labeled cells by cellular MRI. *Eur J Radiol.* 2009;**70**(2):258–64.

9. Rogers WJ, Meyer CH, Kramer CM. Technology insight: in vivo cell tracking by use of MRI. *Nat Clin Pract Cardiovasc Med.* 2006;**3**(10):554–62.

10. Mittal S, Wu Z, Neelavalli J, Haacke EM. Susceptibility-weighted imaging: technical aspects and clinical applications, part 2. *AJNR Am J Neuroradiol.* 2009;**30**(2):232–52.

11. Haacke EM, Mittal S, Wu Z, Neelavalli J, Cheng YC. Susceptibility-weighted imaging: technical aspects and clinical applications, part 1. *AJNR Am J Neuroradiol.* 2009;**30**(1):19–30.

12. Cheng JL, Yang YJ, Li HL, Wang J, Wang MH, Zhang Y. In vivo tracing of superparamagnetic iron oxide-labeled bone marrow mesenchymal stem cells transplanted for traumatic brain injury by susceptibility weighted imaging in a rat model. *Chin J Traumatol.* 2010;**13**(3):173–7.

13. Jisung J, Kwak BK, Reddy AM, Ha BC, Shim HJ, Byun JS, et al. Characterization of Photothrombotic Cerebral Infarction Model At Sensorimotor Area of Functional Map in Rat. *J Neurol Sci (Turkish).* 2013;**30**(4):617–28.

14. Kuroiwa T, Xi G, Hua Y, Nagaraja TN, Fenstermacher JD, Keep RF. Brain edema and blood-brain barrier opening after photothrombotic ischemia in rat. *Acta Neurochir Suppl.* 2013;**118**:11–5.

15. Byun JS, Kwak BK, Kim JK, Jung J, Ha BC, Park S. Engraftment of human mesenchymal stem cells in a rat photothrombotic cerebral infarction model : comparison of intra-arterial and intravenous infusion using MRI and histological analysis. *J Korean Neurosurg Soc.* 2013;**54**(6):467–76.

16. Stroh A, Faber C, Neuberger T, Lorenz P, Sieland K, Jakob PM, et al. In vivo detection limits of magnetically labeled embryonic stem cells in the rat brain using high-field (17.6 T) magnetic resonance imaging. *Neuroimage.* 2005;**24**(3):635–45.

17. Magnitsky S, Watson DJ, Walton RM, Pickup S, Bulte JW, Wolfe JH, et al. In vivo and ex vivo MRI detection of localized and disseminated neural stem cell grafts in the mouse brain. *Neuroimage.* 2005;**26**(3):744–54.

18. Babikian T, Freier MC, Tong KA, Nickerson JP, Wall CJ, Holshouser BA, et al. Susceptibility weighted imaging: neuropsychologic outcome and pediatric head injury. *Pediatr Neurol.* 2005;**33**(3):184–94.

19. Walczak P, Zhang J, Gilad AA, Kedziorek DA, Ruiz-Cabello J, Young RG, et al. Dual-modality monitoring of targeted intraarterial delivery of mesenchymal stem cells after transient ischemia. *Stroke.* 2008;**39**(5):1569–74.

20. Shen LH, Li Y, Chen J, Zhang J, Vanguri P, Borneman J, et al. Intracarotid transplantation of bone marrow stromal cells increases axon-myelin remodeling after stroke. *Neuroscience.* 2006;**137**(2):393–9.

21. Li L, Jiang Q, Ding G, Zhang L, Zhang ZG, Li Q, et al. Effects of administration route on migration and distribution of neural progenitor cells transplanted into rats with focal cerebral ischemia, an MRI study. *J Cereb Blood Flow Metab.* 2010;**30**(3):653–62.

22. Deistung A, Dittrich E, Sedlacik J, Rauscher A, Reichenbach JR.

ToF-SWI: simultaneous time of flight and fully flow compensated susceptibility weighted imaging. *J Magn Reson Imaging.* 2009;**29**(6):1478–84.

23. Chavhan GB, Babyn PS, Thomas B, Shroff MM, Haacke EM. Principles, techniques, and applications of T2*-based MR imaging and its special applications. *Radiographics.* 2009;**29**(5):1433–49.

24. Zulfiqar M, Dumrongpisutikul N, Intrapiromkul J, Yousem DM. Detection of intratumoral calcification in oligodendrogliomas by susceptibility-weighted MR imaging. *AJNR Am J Neuroradiol.* 2012;**33**(5):858–64.

25. Bulte JW, Walczak P, Gleich B, Weizenecker J, Markov DE, Aerts HC, et al. MPI Cell Tracking: What Can We Learn from MRI? *Proc Soc Photo Opt Instrum Eng.* 2011;**7965**:79650z.

26. Karussis D, Karageorgiou C, Vaknin-Dembinsky A, Gowda-Kurkalli B, Gomori JM, Kassis I, et al. Safety and immunological effects of mesenchymal stem cell transplantation in patients with multiple sclerosis and amyotrophic lateral sclerosis. *Arch Neurol.* 2010;**67**(10):1187–94.